5518 *Biochemistry* **2009,** *48,* 5518–5531
DOI: 10.1021/bi900623r

BIOCHEMISTRY
including biophysical chemistry & molecular biology
Article

Mechanism of the Orotidine 5′-Monophosphate Decarboxylase-Catalyzed Reaction: Evidence for Substrate Destabilization[†,‡]

Kui K. Chan,[§] B. McKay Wood,[§] Alexander A. Fedorov,[∥] Elena V. Fedorov,[∥] Heidi J. Imker,[§] Tina L. Amyes,[⊥] John P. Richard,[⊥] Steven C. Almo,*[,∥] and John A. Gerlt*[,§]

[§]*Departments of Biochemistry and Chemistry, University of Illinois at Urbana−Champaign, Urbana, Illinois 61801,* [∥]*Department of Biochemistry, Albert Einstein College of Medicine, Bronx, New York 10461, and* [⊥]*Department of Chemistry, University at Buffalo, Buffalo, New York 14260*

Received April 10, 2009; Revised Manuscript Received May 11, 2009

ABSTRACT: The reaction catalyzed by orotidine 5′-monophosphate decarboxylase (OMPDC) involves a stabilized anionic intermediate, although the structural basis for the rate acceleration (k_{cat}/k_{non}, 7.1×10^{16}) and proficiency [$(k_{cat}/K_M)/k_{non}$, 4.8×10^{22} M^{-1}] is uncertain. That the OMPDCs from *Methanothermobacter thermautotrophicus* (MtOMPDC) and *Saccharomyces cerevisiae* (ScOMPDC) catalyze the exchange of H6 of the UMP product with solvent deuterium allows an estimate of a lower limit on the rate acceleration associated with stabilization of the intermediate and its flanking transition states ($\geq 10^{10}$). The origin of the "missing" contribution, $\leq 10^7$ ($\sim 10^{17}$ total $- \geq 10^{10}$), is of interest. Based on structures of liganded complexes, unfavorable electrostatic interactions between the substrate carboxylate group and a proximal Asp (Asp 70 in MtOMPDC and Asp 91 in ScOMPDC) have been proposed to contribute to the catalytic efficiency [Wu, N., Mo, Y., Gao, J., and Pai, E. F. (2000) *Proc. Natl. Acad. Sci. U.S.A. 97*, 2017−2022]. We investigated that hypothesis by structural and functional characterization of the D70N and D70G mutants of MtOMPDC and the D91N mutant of ScOMPDC. The substitutions for Asp 70 in MtOMPDC significantly decrease the value of k_{cat} for decarboxylation of FOMP (a more reactive substrate analogue) but have little effect on the value of k_{ex} for exchange of H6 of FUMP with solvent deuterium; the structures of wild-type MtOMPDC and its mutants are superimposable when complexed with 6-azaUMP. In contrast, the D91N mutant of ScOMPDC does not catalyze exchange of H6 of FUMP; the structures of wild-type ScOMPDC and its D91N mutant are not superimposable when complexed with 6-azaUMP, with differences in both the conformation of the active site loop and the orientation of the ligand vis á vis the active site residues. We propose that the differential effects of substitutions for Asp 70 of MtOMPDC on decarboxylation and exchange provide additional evidence for a carbanionic intermediate as well as the involvement of Asp 70 in substrate destabilization.

As nature's most proficient enzyme, orotidine 5′-monophosphate decarboxylase (OMPDC)[1] has attracted considerable attention among mechanistic enzymologists (Scheme 1). In 1995, Wolfenden quantitated the extraordinary rate acceleration, 1.4×10^{17} ($k_{cat} = 39$ s^{-1}; $k_{non} = 2.8 \times 10^{-16}$ s^{-1}), and proficiency, [$(k_{cat}/K_M)/k_{non}$], 2.0×10^{23} M^{-1} ($k_{cat}/K_M = 5.6 \times 10^7$ M^{-1} s^{-1}), for the OMPDC from *Saccharomyces cerevisiae* (ScOMPDC) (*2*).[2] Since that time, the challenge has been to understand the catalytic prowess in terms of active site structure (*3*). However, despite the availability of high-resolution structures and

[†]This research was supported by NIH Grants GM039754 (to J.P.R.) and GM065155 (to J.A.G.). Molecular graphics images were produced using the UCSF Chimera package from the Resource for Biocomputing, Visualization, and Informatics at the University of California, San Francisco (supported by NIH Grant P41 RR-01081).

[‡]The X-ray coordinates and structure factors for the following structures have been deposited in the Protein Data Bank with the indicated accession codes: wild-type MtOMPDC in the absence of ligands (PDB accession code 3G18), wild-type MtOMPDC complexed with 6-azaUMP (3G1A), wild-type MtOMPDC complexed with UMP (3G1D), wild-type MtOMPDC complexed with H2OMP (3G1F), wild-type MtOMPDC complexed with H2UMP (3G1H), the D70N mutant of MtOMPDC in the absence of ligands (3G1Y), the D70N mutant of MtOMPDC complexed with 6-azaUMP (3G24), the D70N mutant of MtOMPDC complexed with UMP (3G22), the D70G mutant of MtOMPDC in the absence of ligands (3G1S), the D70G mutant of MtOMPDC complexed with UMP (3G1X), the D70G mutant of MtOMPDC complexed with FOMP (3G1V), wild-type ScOMPDC in the absence of ligands (3GDK), wild-type ScOMPDC complexed with 6-azaUMP (3GDL), the D91N mutant of ScOMPDC in the absence of ligands (3GDR), and the D91N mutant of ScOMPDC complexed with 6-azaUMP (3GDT).

*To whom correspondence should be addressed. J.A.G.: phone, (217) 244-7414; fax, (217) 244-6538; e-mail, j-gerlt@uiuc.edu. S.C.A.: phone, (718) 430-2746; fax, (718) 430-8565; e-mail, almo@aecom.yu.edu.

[1]Abbreviations: FOMP, 5-fluoroorotidine 5′-monophosphate; FUMP, 5-fluorouridine 5′-monophosphate; azaUMP, 6-azauridine 5′-monophosphate; BMP, 1-(5′-phospho-β-D-ribofuranosyl)barbituric acid; H_2OMP, (6*R*)-5,6-dihydroorotidine 5′-monophosphate; H_2UMP, 5,6-dihydrouridine 5′-monophosphate; MtOMPDC, OMPDC from *Methanothermobacter thermautotrophicus*; OMP, orotidine 5′-monophosphate; OMPDC, orotidine 5′-monophosphate decarboxylase; PIE, product isotope effect; ScOMPDC, OMPDC from *Saccharomyces cerevisiae*; WT, wild type.

[2]Our values for wild-type ScOMPDC: $k_{cat} = 20$ s^{-1}, rate acceleration $= 7.1 \times 10^{16}$; $k_{cat}/K_M = 1.3 \times 10^7$ M^{-1} s^{-1}, proficiency $= 4.6 \times 10^{22}$ M^{-1} (*1*).

Published on Web 05/12/2009

Scheme 1

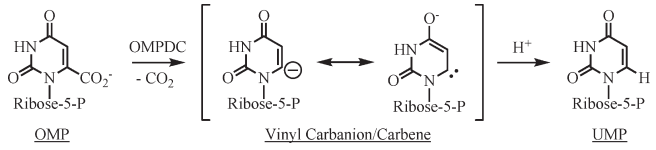

Scheme 2

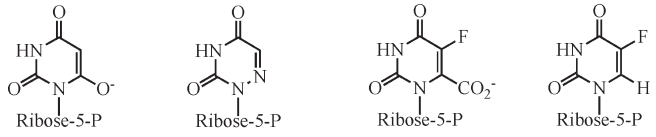

limited kinetic data for mutant enzymes (*vide infra*), little progress has been made in achieving that goal.

Despite significant sequence divergence, the active site structures of OMPDCs are highly conserved (*4*). OMPDCs are obligate dimers of $(\beta/\alpha)_8$ barrels, with the active sites located at the dimer interface. Four divergent subfamilies of OMPDCs can be identified in the sequence databases that differ in the sequence and structure of a loop at the end of the seventh β-strand that closes when substrate binds, "clamping" the substrate within the solvent-sequestered active site (J. A. Gerlt, P. C. Babbitt, and S. Brown, unpublished observations).

In 2000, structures were reported for four OMPDCs (*5*−*8*), including ScOMPDC and the OMPDC from *Methanothermobacter thermautotrophicus* (formerly *Methanobacterium thermoautotrophicum*; MtOMPDC). Subsequently, Wolfenden reported kinetic studies of mutants of ScOMPDC (*9*−*11*), although the only structures of ScOMPDC have been those of the wild-type enzyme in the absence and presence of the competitive inhibitor barbiturate 5′-monophosphate (BMP, an analogue of a carbanionic transition state/intermediate with negative charge localized proximal to C6 of the pyrimidine moiety; Scheme 2) (*5*). Pai reported structures of wild-type MtOMPDC as well as of several mutants of active site residues in the absence and presence of either BMP or 6-azaUMP (also an analogue of a carbanionic transition state/intermediate; Scheme 2), although the kinetic constants of the mutants were not reported (*6*, *12*). In virtually all of the liganded structures that have been reported, C6/N6 of the pyrimidine base is proximal to a hydrogen-bonded Asp-Lys-Asp triad. The active site structure of the 6-azaUMP complex of MtOMPDC (*vide infra*) is shown in Figure 1 (panel A, front view; panel B, side view) with Asp 70, Lys 72, and Asp 75 (from the neighboring polypeptide in the biological dimer) forming the catalytic triad.[3] Lys 72 is thought to deliver a solvent-derived hydrogen to C6 to form the UMP product. But, the roles of the Asp residues are both uncertain and controversial (*13*, *14*), although early speculation focused on destabilization of the OMP carboxylate group by unfavorable electrostatic interactions (*6*, *15*).

Although several mechanisms have been proposed, we recently established that the mechanism is stepwise, involving the formation of a stabilized vinyl carbanion intermediate (Scheme 1): (1) no discrimination between solvent protium and deuterium is observed in the formation of the UMP product (*16*), and (2) H6 of the UMP product undergoes slow exchange with solvent deuterium (*17*). The rate of exchange of H6 of the UMP product with solvent deuterium can be used to estimate its pK_a within the active site. In solution, the pK_a of 1,3-dimethyluracil is estimated as 34 ± 2 (*18*) and 30 (*19*); in the active sites of both ScOMPDC and MtOMPDC, the pK_a of UMP is ≤22 (*17*). The difference establishes that the active site stabilizes the vinyl carbanion by ≥14 kcal/mol (producing a rate acceleration $\geq 10^{10}$). The structural features that provide this stabilization remain uncertain: the proximity of the protonated Lys that delivers the solvent-derived hydrogen to C6 to generate UMP provides electrostatic stabilization, but additional stabilization by interactions of O4 of a carbene resonance structure with active site hydrogen bond donors has been proposed (*20*, *21*) but not experimentally investigated.

The simultaneous reports of the structures of ScOMPDC (*5*), MtOMPDC (*6*), and the OMPDCs from *Bacillus subtilis* (*7*) and *Escherichia coli* (*8*) prompted speculation that the proximity of the substrate carboxylate group to an active site Asp (Asp 70 in MtOMPDC; Asp 91 in ScOMPDC; Figure 1) contributes to the rate acceleration by electrostatic repulsion and/or geometric distortion of the substrate (*6*, *13*, *14*). In support of this proposal, Raman spectroscopic studies of 6-cyanoUMP complexed with ScOMPDC have been interpreted in terms of distortion of the nitrile group out of the plane of the pyrimidine ring (*22*). Perhaps such "substrate destabilization"[4] provides the "missing" factor of $\leq 10^7$ to fully explain the rate acceleration (10^{17} total − $\geq 10^{10}$ from intermediate stabilization). However, the importance of substrate destabilization has not been experimentally evaluated.

Substitutions for an active site residue that participates only in stabilization of the vinyl carbanion intermediate should have similar effects on the rate constants for formation of the carbanion from OMP by decarboxylation and deprotonation of UMP (exchange) in the reverse direction. However, if the effects on the rate constants for decarboxylation and exchange were substantially different, the conclusion would be that the residue plays different roles in stabilizing the transitions states for carbanion formation by the different pathways.

We now report kinetic and structural studies that evaluate the mechanistic roles of Asp 70 in MtOMPDC and its homologue Asp 91 in ScOMPDC. For MtOMPDC, the D70N and D70G substitutions significantly and progressively decrease the value of

[3]As shown in Figure 1, Lys 42 is hydrogen-bonded to Asp 70 in the triad that is proximal to C6/N6 of pyrimidine nucleotide ligands. Lys 42 is also hydrogen-bonded to the 3′-OH group of nucleotide ligands; the position and conformation of Lys 42 are independent of the identity of residue 70 (*vide infra*).

[4]The term "ground state destabilization" is used to describe an interaction between the active site and substrate that destabilizes the Michaelis complex and, therefore, increases the value of K_M relative to an environment in which the unfavorable interaction is not present. If the unfavorable interaction is relieved in the transition state, the amount of destabilization will be expressed as an equivalent increase in the value of k_{cat}. Therefore, the value of k_{cat}/K_M will be the same in the presence and absence of the interaction if "ground state destabilization" is important. The data presented in this paper do not conform to this definition of "ground state destabilization", perhaps because the destabilizing interactions are not fully expressed in a "Michaelis complex" but develop as the reaction coordinate from an initial encounter complex is traversed. This suggests the importance of conformational changes/dynamics in catalysis, evidence for which is obtained by comparing the structures of both MtOMPDC and ScOMPDC in the absence and presence of transition state/intermediate analogues, as described in this paper. We use the term "substrate destabilization" instead of "ground state destabilization" to describe the effects of substitutions for Asp 70 in MtOMPDC on the kinetic constants.

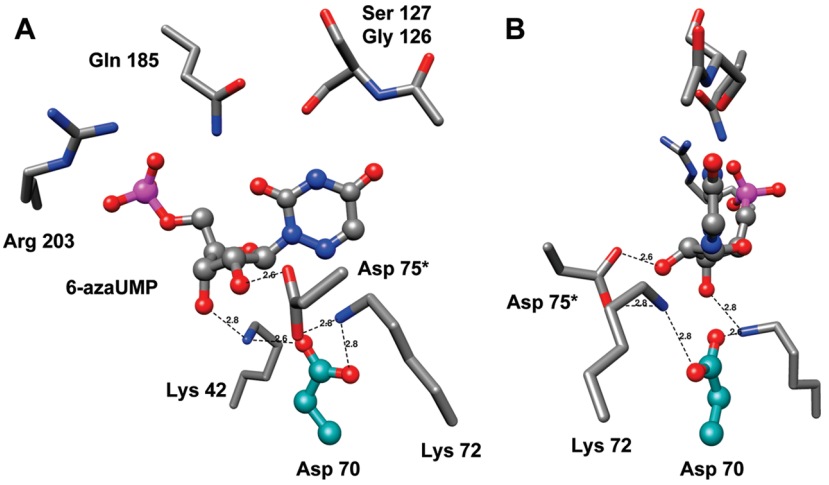

FIGURE 1: Active site of wild-type MtOMPDC complexed with 6-azaUMP. Panel A: front view, with Asp 75 from the second polypeptide marked with an asterisk. Panel B: side view.

k_{cat} for decarboxylation of OMP and FOMP (a more reactive substrate analogue; Scheme 2) but have little effect on the value of k_{ex} for exchange of H6 of the FUMP product with solvent deuterium; the structures of the active sites of wild-type MtOMPDC and its D70N and D70G mutants are virtually superimposable when complexed with 6-azaUMP. These results establish that the Asp-Lys-Asp triad functions differently in the decarboxylation and exchange reactions, providing additional evidence for a carbanion intermediate and suggesting the involvement of Asp 70 in destabilization of the substrate.

In unexpected contrast, the D91N mutant of ScOMPDC is not an effective catalyst for either decarboxylation of FOMP or exchange of H6 of FUMP. Also, the structures of the active sites of wild-type ScOMPDC and its D91N mutant are not superimposable when complexed with 6-azaUMP, with striking differences in both the conformation of the active site loop and the orientation of the ligand vis á vis the active site residues. These structural differences show that ScOMPDC can form two different complexes with ligands: (1) a "crowded," catalytically productive complex in which the substrate carboxylate group and the Asp-Lys-Asp triad are in forced proximity and (2) a more "commodious," loop-open complex that can accommodate bulky ligands with binding constants comparable to those for OMP and UMP (*23*).

MATERIALS AND METHODS

Materials. ^{1}H and ^{19}F NMR spectra were recorded using a Varian INOVA 500NB NMR spectrometer (500 MHz for ^{1}H and 470 MHz for ^{19}F). OMP and FOMP were prepared as described in the preceding paper (*1*). 6-AzaUMP was purchased from R.I. Chemical Inc. All other reagents were purchased from Sigma Aldrich at the highest purity available. All solutions were prepared with Millipore Ultrapure filtered water.

Synthesis of 5,6-Dihydrouridine 5′-Monophosphate (H$_2$UMP). UMP (500 mg, 1.36 mmol) was dissolved in 10 mL of H_2O, and 10 mL of methanol was added. After addition of 5% palladium on activated carbon (200 mg), the reduction was performed in a Parr shaker under 35 psi pressure of H_2. The reaction was allowed to continue for 24 h; complete reduction of the pyrimidine moiety was confirmed by disappearance of the absorbance at 268 nm. The reaction mixture was filtered to remove the catalyst, and the solvent was removed by rotary evaporation to yield a clear, colorless syrup. The material was dissolved in a small volume of H_2O; the concentration was determined by Ames phosphate analysis (*24*). Purity was confirmed by ^{1}H NMR.

H_2UMP: ^{1}H NMR (D_2O, 500 MHz): δ (ppm) 5.7 (d, H-1′), 4.3 (dd, H-2′), 4.2 (dd, H-3′), 4.0 (m, H-4′), 3.7 (t, H-6), 3.6−3.4 (ABX, H-5′), and 2.6 (t, H-5).

Synthesis of 5,6-Dihydroorotidine 5′-Monophosphate (H$_2$OMP). OMP (40 mg, 0.1 mmol) was dissolved in 6 mL of H_2O, and 6 mL of methanol was added. After addition of 5% palladium on activated carbon (21 mg), the reduction was performed in a Parr shaker under 40 psi pressure of H_2. After 24 h, complete reduction was confirmed by disappearance of the absorbance at 279 nm. The reaction mixture was filtered and concentrated to dryness. The residue was dissolved in a small volume of H_2O; the concentration was determined by Ames phosphate analysis.

Inspection of the ^{1}H NMR spectrum revealed production of only one diastereomer of H_2OMP (a chiral center is generated at C-6 of the dihydropyrimidine ring). Given the preference for OMP to adopt the syn conformation (*25*), assignment of the 6-*R* configuration to C-6 was determined by a standard one-dimensional NOESY experiment. A strong NOE was observed between H-6 and H-2′, and weak NOEs were observed between H-6 and both H-1′ and H-2′, consistent with the 6-*R* configuration. No NOEs were observed between H-6 and the remaining protons.

H_2OMP: ^{1}H NMR (D_2O, 500 MHz): δ (ppm) 5.8 (d, H-1′), 4.2 (dd, H-6), 4.1 (dd, H-2′), 4.0 (dd, H-3′), 3.9 (m, H-4′), 3.8−3.6 (m, H-5′), and 3.0−2.7 (ABX, H-5).

Synthesis of FUMP. The procedure of Fujita et al. was followed with modifications (*26*). Phosphorus oxychloride (330 μL) was added under dry nitrogen to a stirred mixture of 5-fluorouridine (1.9 mmol) and 5 mL of anhydrous trimethyl phosphate. After 16 h at 4 °C, the reaction was quenched with 100 mL of H_2O. Sodium hydroxide (18 mmol) was added, and the solution was loaded onto a DEAE-Sepharose Fast Flow column (2.5 × 25 cm; HCO_3^-); unreacted 5-fluorouridine was washed from the column with 500 mL of water. FUMP was eluted with a 1 L linear gradient from 0 to 0.25 M triethylammonium bicarbonate, pH 8.4. The product-containing fractions were identified by OD at 269 nm (ε_{269} = 9200 M^{-1} cm^{-1}); ^{1}H NMR spectra of aliquots of fractions were recorded to assess purity. Fractions containing pure FUMP were evaporated; the solid was redissolved in water and taken to dryness several times to remove

Table 1: Data Collection and Refinement Statistics for Complexes of Wild-Type MtOMPDC

	MtOMPDC·apo	MtOMPDC·azaUMP	MtOMPDC·UMP	MtOMPDC·H_2OMP	MtOMPDC·H_2UMP
Data Collection					
space group	$P4_1$	$P2_1$	$P2_1$	$C2$	$C2$
no. of molecules in asym unit	2	2	2	13	13
cell dimensions					
a (Å)	56.85	59.73	59.57	147.61	147.90
b (Å)	56.85	64.14	64.22	101.71	101.80
c (Å)	125.54	61.52	61.82	192.08	192.83
β (deg)		115.36	115.41	91.49	91.59
resolution (Å)	1.6	1.5	1.5	2.5	2.3
no. of unique reflections	52290	66146	65391	94751	126808
R_{merge}	0.048	0.062	0.071	0.078	0.067
$I/\sigma I$	31.4	22.3	15.1	15.9	16.5
completeness (%)	99.9	98.4	97.0	96.4	100
Refinement					
resolution (Å)	25.0−1.6	25.0−1.5	25.0−1.5	25.0−2.5	25.0−2.3
R_{cryst}	0.227	0.187	0.232	0.243	0.242
R_{free}	0.239	0.207	0.258	0.294	0.285
no. of atoms					
protein	3246	3301	3301	21372	21383
waters	193	336	246	73	246
bound ligand		6aza-UMP	UMP	H_2OMP	H_2UMP
ligand atoms		42	42	312	273
rms deviations					
bond lengths (Å)	0.005	0.006	0.006	0.008	0.009
bond angles (deg)	1.43	1.38	1.45	1.4	1.3
PDB entry	3G18	3G1A	3G1D	3G1F	3G1H

excess triethylammonium bicarbonate. The product was dissolved in water and lyophilized to yield the final product (26% yield).

MtOMPDC and ScOMPDC. Wild-type MtOMPDC, the D70N mutant of MtOMPDC, and wild-type ScOMPDC were prepared as described in the preceding paper (*1*). The D70G mutant of MtOMPDC were constructed using the QuikChange II method (Stratagene). DNA sequencing at the University of Illinois Core Sequencing Facility confirmed the expected sequences. The D70G mutant was purified from a *pyr*F$^-$ strain of *E. coli* as described in the preceding paper for the D70N mutant (*1*).

Crystallization and Data Collection. For wild-type MtOMPDC, five different crystal forms were grown by the hanging drop method at room temperature (Table 1): (1) in the absence of a ligand (WT·apo), (2) complexed with 6-azaUMP (WT·azaUMP), (3) complexed with UMP (WT·UMP), (4) complexed with H_2OMP (WT·H_2OMP), and (5) complexed with H_2UMP (WT·H_2UMP). The crystallization conditions utilized the following conditions:

For MtOMPDC·apo, the protein solution contained wild-type MtOMPDC (38 mg/mL) in 20 mM HEPES, pH 7.5, 150 mM NaCl, and 3 mM DTT; the precipitant contained 30% PEG ME 550, 0.1 M HEPES, pH 7.5, and 0.05 M $MgCl_2$. Crystals appeared in 2−3 days and exhibited diffraction consistent with the space group $P4_1$, with two polypeptides per asymmetric unit.

For MtOMPDC·azaUMP, the protein solution contained wild-type MtOMPDC (38 mg/mL) in 20 mM HEPES, pH 7.5, 40 mM azaUMP, 150 mM NaCl, and 3 mM DTT; the precipitant contained 25% PEG 3350, 0.1 M Tris-HCl, pH 8.5, and 0.2 M $MgCl_2$. Crystals appeared in 4 days and exhibited diffraction consistent with space group $P2_1$, with two polypeptides per asymmetric unit.

For MtOMPDC·UMP, the protein solution contained wild-type MtOMPDC (38 mg/mL) in 20 mM HEPES, pH 7.5, 40 mM UMP, 150 mM NaCl, and 3 mM DTT; the precipitant contained 30% PEG 4000, 0.1 M sodium citrate, pH 5.6, and 0.2 M ammonium acetate. Crystals appeared in 4−5 days and exhibited diffraction consistent with space group $P2_1$ with two polypeptides per asymmetric unit.

For MtOMPDC·H_2OMP, the protein solution contained wild-type OMPDC (38 mg/mL) in 20 mM HEPES, pH 7.5, 20 mM H_2OMP, 150 mM NaCl, and 3 mM DTT; the precipitant contained 30% PEG 4000, 0.1 M sodium citrate, pH 5.6, and 0.2 M ammonium acetate. Crystals appeared in 8 days and exhibited diffraction consistent with the space group $C2$, with 13 polypeptides per asymmetric unit.

For MtOMPDC·H_2UMP, the protein solution contained wild-type OMPDC (38 mg/mL) in 20 mM HEPES, pH 7.5, 40 mM H_2UMP, 150 mM NaCl, and 3 mM DTT; the precipitant contained 30% M PEG 4000, 0.1 M sodium citrate, pH 5.6, and 0.2 M ammonium acetate. Crystals appeared in 7−8 days and exhibited diffraction consistent with the space group $C2$ with 13 polypeptides per asymmetric unit.

For the D70N mutant of MtOMPDC, three different crystal forms were grown by the hanging drop method at room temperature (Table 2): (1) complexed with SO_4^{2-} (D70N·SO_4^{2-}), (2) complexed with UMP (D70N·UMP), and (3) complexed with azaUMP (D70N·azaUMP). The crystallization conditions utilized the following conditions:

For D70N·SO_4^{2-}, the protein solution contained the D70N mutant of MtOMPDC (46 mg/mL) in 20 mM HEPES, pH 7.5, 100 mM NaCl, and 3 mM DTT; the precipitant contained 2.0 M $(NH_4)_2SO_4$, 0.1 M HEPES, pH 7.5, and 2% PEG 400. Crystals appeared in 4 days and exhibited diffraction consistent with the space group $P4_1$, with two polypeptides per asymmetric unit.

For D70N·UMP, the protein solution contained the D70N mutant of MtOMPDC (46 mg/mL) in 20 mM HEPES, pH 7.5, 40 mM UMP, 100 mM NaCl, and 3 mM DTT; the precipitant contained 25% PEG 3350, 0.1 M Tris-HCl, pH 8.5, and 0.2 M

Table 2: Data Collection and Refinement Statistics for Complexes of the D70N and D70G Mutants of MtOMPDC

	D70N·SO_4^{2-}	D70N·UMP	D70N·azaUMP	D70G·apo	D70G·UMP	D70G·FUMP
Data Collection						
space group	$P4_1$	$P2_1$	$P2_1$	$P4_1$	$P4_1$	$P4_1$
no. of molecules in asym unit	2	2	2	2	2	2
cell dimensions						
a (Å)	56.57	59.51	59.59	56.76	56.42	56.62
b (Å)	56.57	63.71	63.78	56.76	56.42	56.62
c (Å)	127.35	61.36	61.29	125.75	127.51	127.44
β (deg)		114.94	115.03			
resolution (Å)	1.4	1.5	1.5	1.4	1.55	1.3
no. of unique reflections	78075	61657	60695	77807	56206	90642
R_{merge}	0.069	0.075	0.083	0.064	0.081	0.076
$I/\sigma I$	32.8	25.9	18.6	31.6	23.3	30.9
completeness (%)	99.4	92.5	91.0	99.6	97.5	92.3
Refinement						
resolution (Å)	25.0−1.4	25.0−1.5	25.0−1.5	25.0−1.4	25.0−1.55	25−1.3
R_{cryst}	0.229	0.186	0.183	0.224	0.189	0.193
R_{free}	0.246	0.201	0.197	0.242	0.202	0.211
no. of atoms						
protein	3138	3302	3302	3198	3322	3222
waters	241	291	300	330	198	281
bound ligand	SO_4^{2-}	UMP	6aza-UMP		UMP, Cl^-	FUMP, Cl^-
ligand atoms	10	42	42		42, 2	44, 2
rms deviations						
bond lengths (Å)	0.005	0.005	0.005	0.005	0.005	0.005
bond angles (deg)	1.11	1.20	1.19	1.10	1.20	1.31
PDB entry	3G1Y	3G22	3G24	3G1S	3G1X	3G1V

$MgCl_2$. Crystals appeared in 6 days and exhibited diffraction consistent with space group $P2_1$, with two polypeptides per asymmetric unit.

For D70N·6-azaUMP, the protein solution contained the D70N mutant of MtOMPDC (46 mg/mL) in 20 mM HEPES, pH 7.5, 40 mM 6-azaUMP, 100 mM NaCl, and 3 mM DTT; the precipitant contained 25% PEG 3350, 0.1 M Tris-HCl, pH 8.5, and 0.2 M $MgCl_2$. Crystals appeared in 6 days and exhibited diffraction consistent with space group $P2_1$, with two molecules of D70N OMPDC per asymmetric unit.

For the D70G mutant of MtOMPDC, three different crystal forms were grown by the hanging drop method at room temperature (Table 2): (1) in the absence of a ligand (D70G·apo), (2) complexed with UMP (D70G·UMP), and (3) complexed with FUMP (D70G·FUMP). The crystallization conditions utilized the following conditions:

For D70G·apo, the protein solution contained D70G OMPDC (35 mg/mL) in 20 mM HEPES (pH 7.5), 150 mM NaCl, and 3 mM DTT; the precipitant contained 4.0 M sodium formate, pH 7.0. Crystals appeared in 2 days and exhibited diffraction consistent with the space group $P4_1$, with two polypeptides per asymmetric unit.

For D70G·UMP, the protein solution contained the D70G mutant of MtOMPDC (35 mg/mL) in 20 mM HEPES, pH 7.5, 40 mM UMP, 150 mM NaCl, and 3 mM DTT; the precipitant contained 1.8 M triammonium citrate, pH 7.0. Crystals appeared in 6 days and exhibited diffraction consistent with space group $P4_1$, with two polypeptides per asymmetric unit.

For D70G·FUMP, the protein solution contained the D70G mutant of MtOMPDC (35 mg/mL) in 20 mM HEPES, pH 7.5, 40 mM FUMP, 150 mM NaCl, and 3 mM DTT; the precipitant contained 0.3 M magnesium formate and 0.1 M Bis-Tris, pH 5.5. Crystals appeared in 9 days and exhibited diffraction consistent with space group $P4_1$, with two polypeptides per asymmetric unit.

For wild-type ScOMPDC, two different crystal forms were grown by the hanging drop method at room temperature (Table 3): (1) in the absence of a ligand (ScOMPDC·apo) and (2) and complexed with 6-azaUMP (ScOMPDC·azaUMP).

For ScOMPDC·apo, the protein solution contained wild-type OMPDC (29 mg/mL) in 20 mM Tris, pH 7.9, 100 mM NaCl, and 20% glycerol; the precipitant contained 30% PEG 4000, 0.1 M Tris, pH 8.5, and 0.2 M sodium acetate. Crystals appeared in 4−5 days and exhibited diffraction consistent with the space group $P2_12_12_1$, with four polypeptides per asymmetric unit.

For ScOMPDC·azaUMP, the protein solution contained wild-type OMPDC (29 mg/mL) in 20 mM Tris, pH 7.9, 100 mM NaCl, 20% glycerol, and 40 mM 6-azaUMP; the precipitant contained 30% PEG 2000, 0.1 M sodium acetate, pH 4.6, and 0.2 M ammonium sulfate. The crystals appeared in 9 days and exhibited diffraction consistent with the space group $C2$, with two polypeptides per asymmetric unit.

For the D91N mutant of ScOMPDC, two different crystal forms were grown by the hanging drop method at room temperature (Table 3): (1) in the absence of a ligand (D91N·apo) and (2) and complexed with 6-azaUMP (D91N·azaUMP).

For D91N·apo, the protein solution contained the D91N mutant of ScOMPDC (27 mg/mL) in 50 mM Tris, pH 7.0, and 5% glycerol; the precipitant contained 25% PEG 3350, 0.1 M Bis-Tris, pH 6.5, and 0.2 M $MgCl_2$. Crystals appeared in 4 days and exhibited a diffraction pattern consistent with space group $P2_12_12_1$, with four polypeptides per asymmetric unit.

For D91N·azaUMP, the protein solution contained the D91N mutant of ScOMPDC (27 mg/mL) in 50 mM Tris, pH 7.0, 5% glycerol, and 40 mM 6-azaUMP; the precipitant contained 25% M PEG 3350, and 0.1 M Bis-Tris, pH 5.5. Crystals appeared in 2 weeks and exhibited diffraction consistent with the space group $P2_12_12_1$, with four polypeptides per asymmetric unit.

Prior to data collection, crystals were transferred to cryoprotectant solutions composed of their mother liquids containing

Table 3: Data Collection and Refinement Statistics for Complexes of Wild-Type and the D91N Mutant of ScOMPDC

	ScOMPDC·apo	ScOMPDC·azaUMP	D91N·apo	D91N·azaUMP
Data Collection				
space group	$P2_12_12_1$	$C2$	$P2_12_12_1$	$P2_12_12_1$
no. of molecules in asym unit	4	2	4	4
cell dimensions				
a (Å)	84.13	120.73	84.12	84.35
b (Å)	98.37	80.36	99,14	99.14
c (Å)	127.10	77.57	126.6	126.31
β (deg)		125.12		
resolution (Å)	2.0	1.65	1.9	1.6
no. of unique reflections	71799	69598	83436	139699
R_{merge}	0.053	0.067	0.074	0.081
$I/\sigma I$	28.3	18.2	20.4	27.5
completeness (%)	99.9	95.5	99.3	99.9
Refinement				
resolution (Å)	25.0−2.0	25.0−1.65	25.0−1.9	25.0−1.6
R_{cryst}	0.249	0.200	0.253	0.236
R_{free}	0.280	0.227	0.278	0.257
no. of atoms				
protein	7890	3958	7890	7890
waters	426	382	484	533
rms deviations				
bond lengths (Å)	0.006	0.005	0.005	0.005
bond angles (deg)	1.3	1.3	1.2	1.2
bound ligand		6azaUMP		6azaUMP
ligand atoms		42		84
PDB entry	3GDK	3GDL	3GDR	3GDT

20% glycerol and flash-cooled in a nitrogen stream. All data sets were collected at the NSLS X4A beamline (Brookhaven National Laboratory) with an ADSC CCD detector. Diffraction intensities were integrated and scaled with programs DENZO and SCALEPACK (*27*). The data collection statistics are given in Tables 1 and 2.

Structure Determination and Model Refinement. The structures of MtOMPDC and its mutants were solved by molecular replacement with a fully automated molecular replacement pipeline BALBES (*28*), using only diffraction and sequence data as input; partially refined structures were obtained without any manual intervention. Subsequent several iterative cycles of refinement were performed using manual model rebuilding with TOM (*29*), refinement with CNS (*30*), automatic model rebuilding with ARP (*31*), and solvent building with the CCP4 suite (*32*).

In the unliganded structures of wild-type MtOMPDC and the D70N and D70G mutants, the active site loop containing residues 181−189 is disordered. The various liganded structures of wild-type MtOMPDC and its mutants have well-defined density for this loop, which contacts the ligand. The liganded structures have well-ordered density for the ligands in each active site. No residue (other than Gly) lies in disallowed regions of the Ramachandran plot in the structures of wild-type MtOMPDC and its mutants. In each structure, the polypeptides form closed dimers, with the monomers connected by noncrystallographic 2-fold axes.

For ScOMPDC and the D91N mutant, the structures were solved by molecular replacement with a fully automated molecular replacement pipeline BALBES (*28*), using only input diffraction and sequence data. Partially refined structures were obtained from BALBES without any manual intervention. Subsequent iterative cycles of refinement were performed that included manual model rebuilding with TOM (*29*), refinement with CNS (*30*), automatic model rebuilding with ARP (*31*), and solvent building with the CCP4 suite (*32*).

In the unliganded structures of wild-type ScOMPDC and the D91N mutant, residues 205−218 in the active site loop are disordered in two of the four molecules in the asymmetric unit and are not included in the final models of these polypeptides; in the polypeptides in which the loop is ordered, this loop is in an "open" conformation. In the ScOMPDC·azaUMP structure, this loop is well-defined in all molecules in the asymmetric unit and is in a "closed" conformation that contacts the 6-azaUMP ligand; the electron density for the ligand is well-defined. In the D91N·azaUMP structure, this loop is well-defined in the "open" conformation in two of the four polypeptides in the asymmetric unit and is disordered in the remaining polypeptides; in the polypeptides in which the loop is ordered, the electron density for the ligand is well-defined, except that it bound in a nonproductive conformation that is described in the Results and Discussion section.

No residue (other than Gly) lies in disallowed regions of the Ramachandran plot in the structures of wild-type ScOMPDC and the D91N mutant. In each structure, the polypeptides form closed dimers, with the monomers connected by noncrystallographic 2-fold axes.

Final crystallographic refinement statistics are provided in Tables 1, 2, and 3.

Enzymatic Assays. OMPDC activity was measured at 25 °C as described in the accompanying paper (*1*), except that the buffer concentration was 50 mM and the ionic strength was maintained at 0.1 M with NaCl. The pH dependence of the kinetic constants was determined using the following buffers: acetate, pH 5.0; MES, pH 6.0; MOPS, pH 7.1 and 7.6; HEPES, pH 7.1, 7.6, and 8.2; Tris-HCl, pH 7.6, 8.2, and 8.4; glycylglycine, pH 8.0, 8.2, 8.4, and 8.7; glycine, pH 9.0, 9.3, 9.6, 10.0, and 10.5; CAPS, pH 11.0.

Exchange of H6 of FUMP. Experiments to measure the rate of exchange of H6 of FUMP with solvent deuterium were performed as described by Amyes et al. with modifications (*17*). Spectra (150 scans) were acquired at 25 °C using a sweep width of

1000 Hz, a 90° pulse angle, an acquisition time of 6 s, and a 2 s relaxation delay. Instead of measuring exchange by integrating the intensity of the remaining proton on C6, exchange was measured by integrating the well-resolved ^{19}F resonances associated with [6-^{1}H]FUMP (doublet at −164.1 ppm; J = 6.7 Hz, coupled to H6) and [6-^{2}H]FOMP (singlet at −164.4 ppm). The logarithm of the fraction of [6-^{1}H]FUMP remaining at time t was plotted as a function of time; the negative slope is the observed exchange rate, k_{obs}. The exchange rate, k_{ex},=k_{obs}[FUMP]$_{total}$/[E].

The pH dependence of k_{ex} was measured using different buffers at the following values of pD: MOPS, pD 7.1 and 7.6; glycylglycine, pD 8.1 and 9.3; glycine, pD 10 and 10.5. The concentration of FUMP was determined from its absorbance at 270 nm (ε_{270} = 8914 M^{-1} cm^{-1}, pH 7.1).

Product Isotope Effect (PIE). The reaction (800 μL) was performed in 50/50 (v/v) H_2O/D_2O at 25 °C with 2 mM FOMP in 50 mM MOPS, pL 7.3, with the ionic strength maintained at 0.1 M with NaCl (*16*). When the reaction was completed, the enzyme was removed by centrifugation (Amicon Microcon YM-10), and the solvent was removed by lyophilization. The residue was dissolved in 800 μL of D_2O, and the pD was adjusted to 7.3. A ^{19}F NMR spectrum was recorded; the PIE was calculated from the ratio of the integrations for the resonances associated with [6-^{2}H]- and [6-^{1}H]FUMP (*vide supra*).

Molecular Graphics Images. The images in Figures 2−5 and 8 were constructed using Chimera (*33*).

RESULTS AND DISCUSSION

The studies reported in this paper focus on the roles of homologous Asp residues in the active site hydrogen-bonded networks in MtOMPDC (Asp 70) and ScOMPDC (Asp 91). The mechanisms of the reactions catalyzed by these homologous OMPDCs have been controversial, so we studied both enzymes to assess whether we would obtain consistent mechanistic inferences. The residues that form the active site are strictly conserved despite the low sequence identity shared by these homologous proteins (~20% from a sequence-based alignment). However, this expectation was not realized, reinforcing the limitations of kinetic and mechanistic studies in the absence of structural information (*vide infra*).

In addition to the natural OMP substrate and UMP product, we used FOMP and FUMP to facilitate our kinetic measurements (Scheme 2). These substrate/product analogues are more reactive than the natural OMP substrate for decarboxylation and the UMP product for exchange of H6 because the electronegative 5-fluoro substituent stabilizes the carbanionic intermediate obtained by decarboxylation of the substrate or abstraction of H6 from the product, respectively. Shostak and Jones reported that the value of k_{cat} for decarboxylation of FOMP by ScOMPDC exceeds that for OMP by 30-fold, although the values of k_{cat}/K_M are the equivalent for OMP and FOMP (*34*). Cleland and co-workers confirmed that FOMP is a better substrate for ScOMPDC, with the increase in k_{cat} reported as 11-fold (*35*). Although not discussed by either Jones or Cleland, the equivalent values for k_{cat}/K_M for decarboxylation of OMP and FOMP (~1 × 10^7 M^{-1} s^{-1}) by ScOMPDC are consistent with rate-limiting substrate binding for one or both substrates. Also, that the values of k_{cat} for OMP and FOMP differ by ~11-fold is consistent with rate-limiting product dissociation, not decarboxylation, for one or both substrates. A measure of the intrinsic effect of 5-fluorine substitution on decarboxylation may be provided by the 350-fold difference in the values of k_{cat} for decarboxylation of OMP and FOMP catalyzed by the D70N mutant of MtOMPDC (*vide infra*); for D70N the values of k_{cat} for both OMP and FOMP are independent of solvent viscosity, so k_{cat} measures the rate of the decarboxylation reaction.

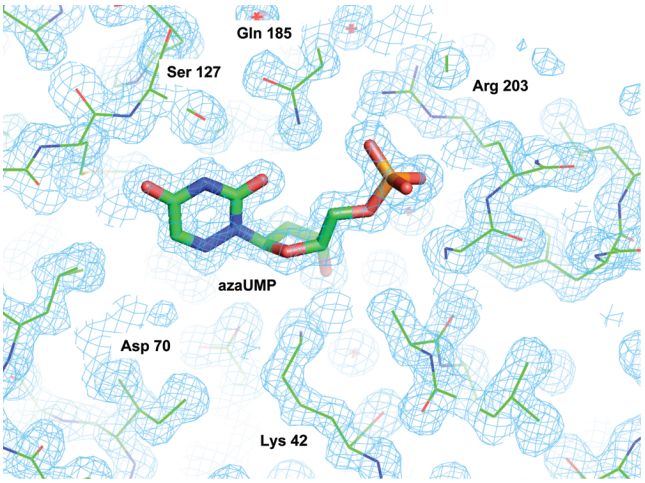

FIGURE 2: Representative electron density for the active site of wild-type MtOMPDC complexed with 6-azaUMP and contoured at 1.5σ. The details of the interactions between 6-azaUMP and the active site are described in the text.

As described in the accompanying paper, the values of k_{cat} measured with FOMP for MtOMPDC and with both OMP and FOMP for ScOMPDC are dependent on solvent viscosity so they are influenced by product dissociation and, therefore, do not directly measure the rate of decarboxylation (*1*). For both enzymes and substrates the values of k_{cat}/K_M also are dependent on solvent viscosity so these kinetic constants include contributions from substrate binding. Recognition that the values of the kinetic constants for both OMP and FOMP can depend on the physical steps of substrate binding and product dissociation is important for interpreting the effects of substitutions of active site residues on mechanism.

Structural Characterization of Wild-Type MtOMPDC. Pai and co-workers reported structures of unliganded wild-type MtOMPDC (1DV7) and the complex with 6-azaUMP (1DVJ), a transition state/intermediate analogue (*12*). We also determined structures of unliganded wild-type MtOMPDC (1.6 Å resolution; 3G18) and its complex with 6-azaUMP (1.5 Å resolution; 3G1A); representative electron density of the 6-azaUMP ligand is presented in Figure 2. Although our structures are essentially identical to those determined by Pai [0.53 Å rmsd for 209 C_α pairs in the unliganded structures (1DV7) and 0.37 Å rmsd for 215 C_α pairs in the liganded structures (1DVJ)], we discovered that the Pai's unliganded structure was solved assuming an incorrect space group ($P4_12_12$), with the correct space ($P4_1$) the same as that we determined. The major difference between our unliganded structure and that determined by Pai is the geometry of the contact between Phe 100 in the two polypeptides at the interface in the functional dimer.

We also determined structures of wild-type MtOMPDC complexed with the UMP product (1.5 Å resolution; 3G1D), (6*R*)-H_2OMP (a distorted substrate analogue; 2.5 Å resolution; 3G1F), and H_2UMP (a distorted product analogue; 2.3 Å resolution; 3G1H). (6*R*)-H_2OMP, with a tetrahedral geometry at C6 (and C5), might be considered an analogue of a destabilized OMP substrate, although the mechanistic importance of out-of-plane distortion of the carboxylate group is uncertain because

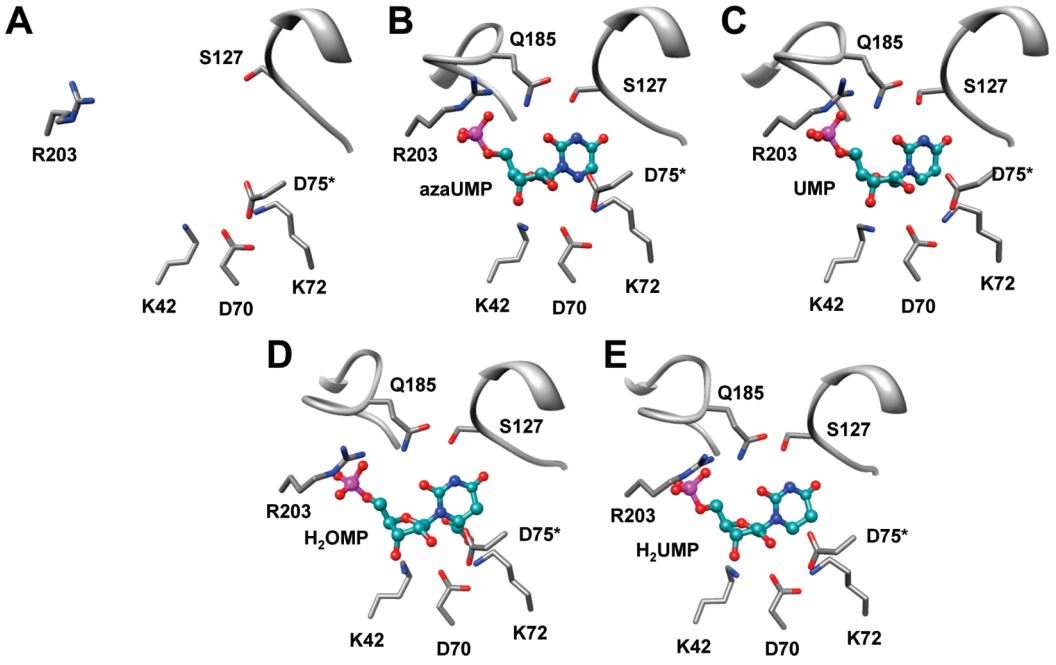

FIGURE 3: Structures of wild-type MtOMPDC in the absence and complexed with ligands. Panel A: in the absence of ligands. Panel B: complexed with 6-azaUMP. Panel C: complexed with UMP. Panel D: complexed with H_2OMP. Panel E: complexed with H_2UMP.

the electron pair of the carbanionic intermediate that resides on C6 is located in an sp^2 orbital in the plane of the pyrimidine ring.

In the unliganded structure, the active site loop (residues 181−189) is disorderd; in all four liganded structures (WT·azaUMP, WT·UMP, WT·H_2OMP, and WT·H_2UMP), the loop is ordered and closed over the ligand to sequester the ligand from solvent (Figure 3, panel A, is the unliganded structure; panels B−E are the structures of the WT·azaUMP, WT·UMP, WT·H_2OMP, and WT·H_2UMP complexes, respectively). The structures of the four complexes superimpose well, although the structures of the backbones of the polypeptides of the liganded structures show small, but significant, differences when compared with that of the unliganded enzyme. Although coupling of substrate binding to catalysis has not been investigated with MtOMPDC as it has with ScOMPDC (*9*, *36*−*38*), conformational changes that accompany substrate binding presumably transmit the substrate's binding energy to the active site where it can be used for substrate destabilization and/or transition state/intermediate stabilization. In each complex, O2 of the pyrimidine ring of the ligand is hydrogen-bonded to the carboxamide group of Gln 185, O4 is hydrogen-bonded to the backbone amide of Ser 127, and N3 is hydrogen-bonded to the OH group of Ser 127.

Structural Characterization of Wild-Type MtOMPDC Liganded with (6R)-H_2OMP. Wolfenden reported that a mixture of diastereomers of H_2OMP (of unspecified diastereomeric composition) is an effective inhibitor of ScOMPDC (K_i = 2.5×10^{-7} M) (*3*). Within the limits of our NMR analyses, we obtained only the (6*R*)-diastereomer by catalytic hydrogenation of OMP (configuration assessed by NOEs between H6 of the reduced pyrimidine ring and the ribose protons; data not shown).

We determined that (6*R*)-H_2OMP is a weak inhibitor of both ScOMPDC and MtOMPDC (K_i, 80 and 100 μM, respectively; data not shown). We also were able to determine the structure of its complex with MtOMPDC but not ScOMPDC. Perhaps the (6*S*)-diastereomer is a more potent inhibitor, although we regard this as unlikely because the 6-carboxylate would be located in a spatially more congested region of the active site, i.e., juxtaposed to the hydrogen-bonded triad (*vide supra*). In the absence of the experimental procedure for Wolfenden's preparation of H_2OMP and, also, his procedures for measurement of the kinetic constants, we cannot explain this apparent kinetic discrepancy. H_2UMP was analogously prepared from UMP; the structure of its complex with MtOMPDC provides an independent assessment of the effect of reduction of the pyrimidine ring on the active site structure.

Both (6*R*)-H_2OMP and H_2UMP are accommodated without perturbation of active site residues relative to their positions in complexes with UMP and 6-azaUMP (Figure 3, panels D and E, respectively). The carboxylate group of (6*R*)-H_2OMP is displaced from the "plane" of the dihydropyrimidine base, as expected from sp^3 hybridization of C6, and is located in a hydrophobic pocket on the opposite face of the active site from Lys 72 (Figure 4, panel A). The carboxylate group does not participate in any hydrogen-bonding/ionic interactions, although disordered water molecules could be located in the hydrophobic pocket. This structure can be compared with that of the inactive D70A/K72A mutant of MtOMPDC complexed with OMP (1KM6) that has been used as evidence for substrate destabilization (Figure 4, panel B). In 1KM6, the carbon of the carboxylate group of the substrate is (1) displaced 0.3 Å out of the plane of the pyrimidine ring, also away from Lys 72, and (2) twisted so that one carboxylate oxygen can be hydrogen-bonded to Lys 42. In the absence of the anionic carboxylate group of Asp 70 and the side chain of Lys 72, no potential unfavorable steric/electrostatic interactions are apparent that would produce the observed out-of-plane distortion of the OMP carboxylate group.

Structural Characterization of the D70N and D70G Mutants of MtOMPDC. We determined structures of the D70N and D70G mutants. Structures were obtained for D70N in the absence of ligands and also complexed with UMP and 6-azaUMP; structures were obtained for D70G in the absence of ligands and complexed with UMP and FUMP. Pai reported structures of D70A complexed with UMP (1KLZ) and D70G complexed with 6-azaUMP (1KLY). As in Pai's structures of D70A (*12*), our structures of D70G contain a chloride ion from the crystallization buffer within the active site, occupying the

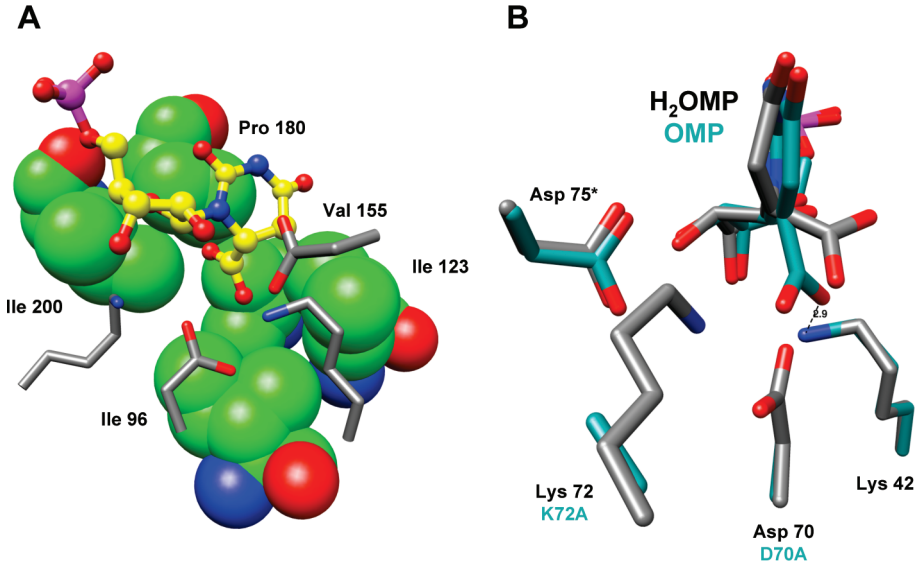

FIGURE 4: Panel A: Front view of active site of wild-type MtOMPDC complexed with H_2OMP, with the side chains of the hydrophobic residues colored in green. Panel B: Side view of the superposition of the active site of wild-type OMPDC complexed with H_2OMP (gray) and of the acive site of the D70A/K72A mutant complexed with OMP (1KM6).

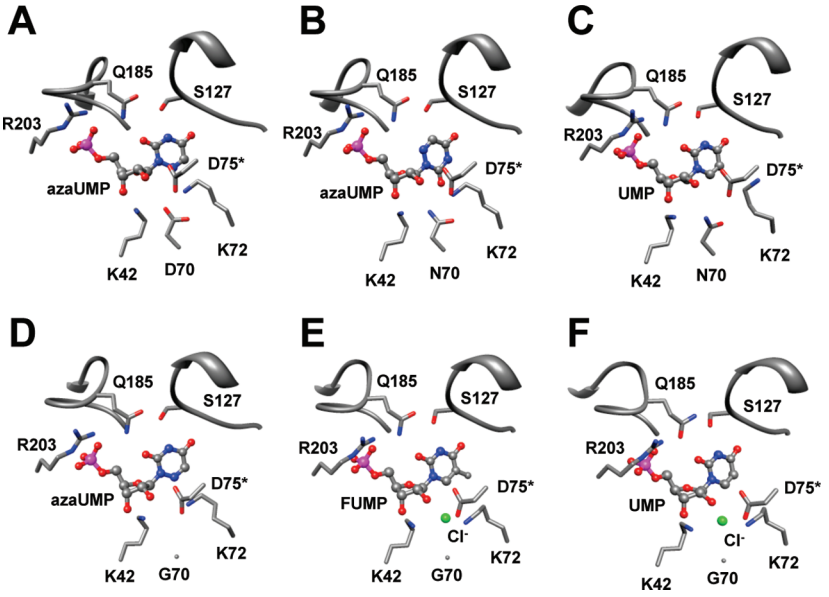

FIGURE 5: Structures of mutants with substitutions for Asp 70. Panel A: wild-type MtOMPDC complexed with 6-azaUMP. Panel B: D70N complexed with 6-azaUMP. Panel C: D70N complexed with UMP. Panel D: D70G complexed with 6-azaUMP. Panel E: D70G complexed with FUMP. Panel F: D70G complexed with UMP. The green spheres represent chloride ions.

position of the carboxylate group of Asp 70 in wild-type MtOMPDC.

In four of the five available structures for D70N and D70G, the nucleotide ligands superimpose closely, with O2 of the pyrimidine ring hydrogen-bonded to Gln 185 [Figure 5, panel A, is the wild-type MtOMPDC liganded with 6-azaUMP; panels B−F are the D70N·azaUMP, D70N·UMP, D70G·6-azaUMP (1KLY), D70G·FUMP, and D70G·UMP complexes, respectively]. The exception is our structure of D70N complexed with 6-azaUMP, in which O2 is hydrogen-bonded to the carboxamide group of Asn 70; i.e., the base is rotated 180° about the glycosidic bond. With the exception of Lys 72, the positions of the active site residues also superimpose closely. Because Asp 70 is hydrogen-bonded to Lys 72 in the active site hydrogen-bonded network, substitution of the Asp carboxymethyl side chain with a neutral and/or sterically less demanding side chain allows Lys 72 to adopt alternate conformations, although in each structure a hydrogen bond is maintained to Asp 75. However, the side chain of Lys 42 remains fixed in the various liganded structures, presumably because of its hydrogen-bonding interaction with O3′ of the ribose moiety of the ligand.

The active sites of D70G complexed with FUMP or UMP but not 6-azaUMP contain a chloride ion located near the position of the carboxylate group of Asp 70 in the wild-type enzyme (*vide infra*). We performed assays of D70G as a function of chloride ion concentration and observed no activation or inhibition, suggesting that the chloride ion is not a functional surrogate of the Asp carboxylate group.

On the basis of these structures, we conclude that significant conformational changes do not accompany the substitutions, thereby allowing the impact of the substitutions on the values of k_{cat} and k_{cat}/K_M to be used to deduce mechanism.

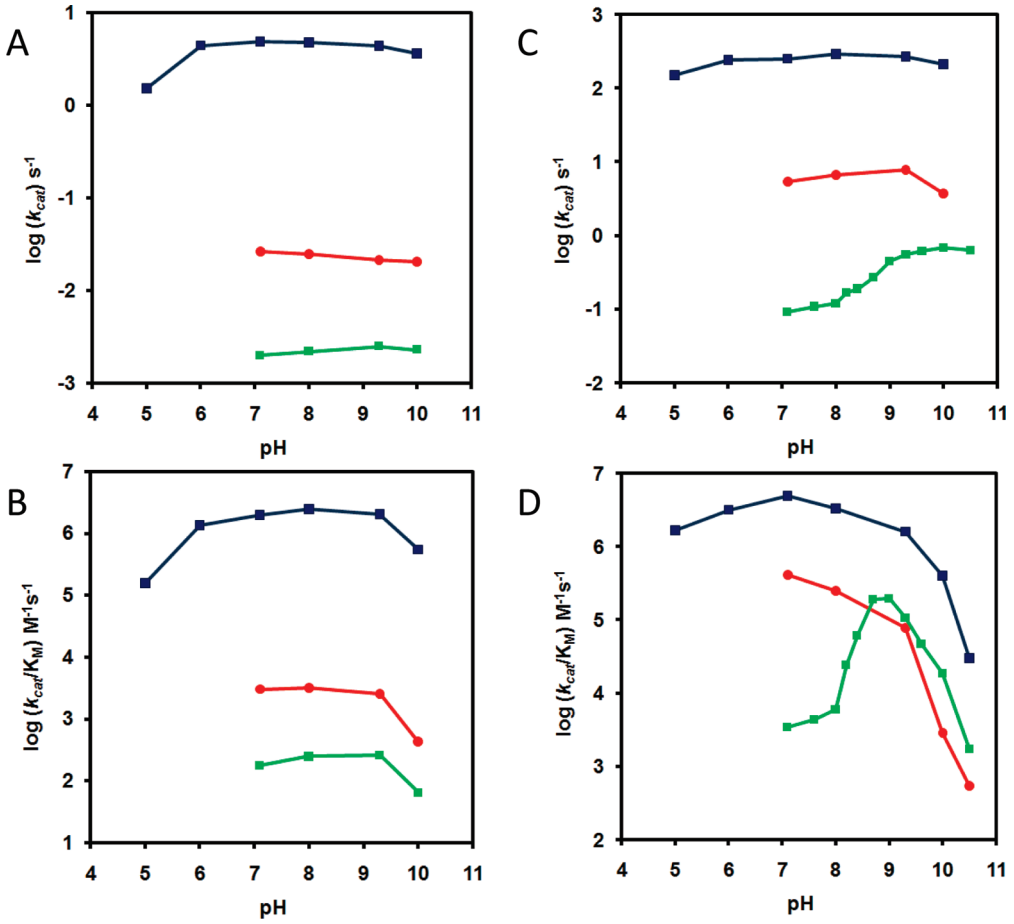

FIGURE 6: Kinetic constants (k_{cat}, panel A; k_{cat}/K_M, panel B) using OMP as substrate for wild-type OMPDC (blue) and its D70N (red) and D70G (green) mutants. Kinetic constants (k_{cat}, panel C; k_{cat}/K_M, panel D) using FOMP as substrate for wild-type OMPDC (blue) and its D70N (red) and D70G (green) mutants.

Table 4: Kinetic Constants for Decarboxylation of OMP and FOMP at pH 9.3 and Exchange of H6 of FUMP

	OMP			FOMP			FUMP
	k_{cat} (s^{-1})	K_M (μM)	k_{cat}/K_M (M^{-1} s^{-1})	k_{cat} (s^{-1})	K_M (μM)	k_{cat}/K_M (M^{-1} s^{-1})	$(k_{ex})_{max}$ (s^{-1})
wild type	4.4 ± 0.1	2.1 ± 0.3	$(2.1 \pm 0.3) \times 10^6$	270 ± 10	170 ± 20	$(1.6 \pm 0.6) \times 10^6$	0.021 ± 0.002
D70N	0.0215 ± 0.0007	8.5 ± 1.3	$(2.5 \pm 0.6) \times 10^3$	7.7 ± 0.2	100 ± 9	$(7.7 \pm 2.2) \times 10^4$	0.009 ± 0.002
D70G	0.0025 ± 0.0008	9.6 ± 0.8	$(2.6 \pm 0.2) \times 10^2$	0.55 ± 0.15	5.1 ± 2.5	$(1.1 \pm 0.4) \times 10^5$	0.030 ± 0.003

Kinetic Characterization of the D70N and D70G Mutants of MtOMPDC: Decarboxylation of OMP and FOMP. Decarboxylation of OMP is the rate-determining energy barrier on the reaction coordinate for wild-type MtOMPDC (the value of k_{cat} is independent of viscosity; the value of k_{cat}/K_M has a small inverse dependence on viscosity) (*1*). However, for FOMP, both k_{cat} and k_{cat}/K_M are inversely proportional to solvent viscosity, so a physical step (substrate binding and product dissociation, respectively) dominates the values of k_{cat} and k_{cat}/K_M. These differences are important for interpreting the kinetic constants.

The pH dependencies of the values of k_{cat} and k_{cat}/K_M for decarboxylation of both OMP and FOMP catalyzed by wild-type MtOMPDC and its D70N and D70G mutants were determined. The data for OMP are displayed in Figure 6, panels A and B; the data for FOMP are displayed in panels C and D. The values of the kinetic constants at pH 9.3 (the pH optimum for D70G with FOMP) are summarized in Table 4.

With OMP, the values of k_{cat} and k_{cat}/K_M decrease in the order wild type > D70N > D70G (the kinetic constants for D70A were not quantitated because enzyme concentrations comparable to substrate concentration were required to observe decarboxylation). The decreases in the values of k_{cat}, 200-fold for D70N and 1800-fold for D70G, provide estimates of the increase in the activation energy barrier as the charge/size of the side chain is neutralized/reduced.

The same qualitative behavior is observed for k_{cat} and k_{cat}/K_M when FOMP is used as substrate, although the values of k_{cat} are pH-dependent for the D70G mutant. The values of k_{cat}/K_M decrease less than the values of k_{cat}, because the values of K_M for the mutants are less than that for wild type. However, with FOMP, the decreases in the value of k_{cat} relative to that for wild type, 35-fold for D70N and 490-fold for D70G, do not provide estimates for the increases in activation energy barrier for decarboxylation, because k_{cat} for wild-type MtOMPDC with FOMP is dominated by production dissociation, not decarboxylation (*1*). Assuming that the ratio of the viscosity-independent values of k_{cat} for decarboxylation of OMP and FOMP catalyzed by D70N ($7.7\ s^{-1}/0.022\ s^{-1} = 350$) reflects the "intrinsic" effect of the 5-fluoro substitution in stabilizing the

carbanion obtained by decarboxylation, we estimate the rate of decarboxylation of FOMP in the active site by wild-type MtOMPDC as 4.4 $s^{-1} \times 350 \approx 1500\ s^{-1}$. With this assumption, the decreases in the rates of decarboxylation are 190-fold for D70N and 2700-fold for D70G. The reductions for D70N and D70G are similar to those measured when OMP is used as substrate (*vide supra*).

We conclude that, irrespective of whether OMP or FOMP is the substrate, large reductions in the rate of decarboxylation are produced by substitution of Asp 70 with neutral and/or smaller residues.

That the values of K_M for both OMP and FOMP are virtually the same for D70N and D70G substitutions is inconsistent with the classical definition of "ground state destabilization"; i.e., the substitutions for Asp 70 decrease the affinity of the enzyme for the substrate in the absence of a destabilizing interaction.[4] A possible explanation is that conformational changes accompany the binding of substrate and subsequent formation of transition state/intermediate/product complexes (*vide infra*); these will contribute to and prevent quantitative interpretation of the value of K_M in the context of changes expected if "ground state destabilization" of a static Michaelis complex were assumed.

Kinetic Characterization of the D70N and D70G Mutants of MtOMPDC: Exchange of H6 of FUMP. Both wild-type ScOMPDC and MtOMPDC catalyze the slow exchange of H6 of UMP with solvent deuterium (*17*). For ScOMPDC, the rate constant for the exchange reaction, k_{ex}, increases with pD, giving values of 8.0 for the pK_a of the base (Lys 93) and $1.2 \times 10^{-5}\ s^{-1}$ for the pH-independent maximum rate $(k_{ex})_{max}$. Measurement of the slow rate of exchange reaction using UMP requires both high concentrations of enzyme and long incubation times (≤250 h). We observed that H6 of FUMP undergoes exchange with solvent deuterium ~3200-fold faster with FUMP than UMP in the presence of wild-type MtOMPDC (*vide infra*) and wild-type ScOMPDC.[5] Therefore, we used FUMP to investigate the exchange reactions catalyzed by wild type and the D70N and D70G mutants of MtOMPDC.

We determined k_{ex} as a function of pD for the wild type and the D70N and D70G mutants of MtOMPDC using 5 mM FUMP. The value of k_{ex} increases with pD and becomes pD independent at high values of pD (Figure 7). The dependence of k_{ex} on [FUMP] was measured at pD 9.3 for all three proteins (where the values of k_{cat} are maximal) and observed to be independent of the concentration of FUMP at 5 mM; the values of $(k_{ex})_{max}$ are collected in Table 4. In contrast to the values of k_{cat} for decarboxylation of FOMP, the values of $(k_{ex})_{max}$ are not significantly influenced by substitutions for Asp 70.

The value of k_{ex} is a composite of the rates of abstraction of H6 to generate the vinyl carbanion intermediate and subsequent delivery of solvent deuterium from Lys 72. Because the solvent product isotope effect (PIE) is 1.0 for wild-type MtOMPDC using both OMP and FOMP, hydron transfer from Lys 72 each of the carbanion intermediates must be faster than rotation of the C_ε−N bond that exchanges the positions of the hydrons (*16*). In wild-type MtOMPDC, hydrogen bonds between Lys 72 and both Asp 70 and Asp 75 may restrict this rotation. Substitutions for Asp 70 that remove or weaken the hydrogen bond to Lys 72 could allow enhanced rotation so that it could be faster than hydron transfer; as a result, the same value of k_{ex} could be obtained if the

[5]W.-Y. Tsang, T. L. Amyes, B. M. Wood, K. Chan, W. Wu, J. A. Gerlt, and J. P. Richard, manuscript in preparation.

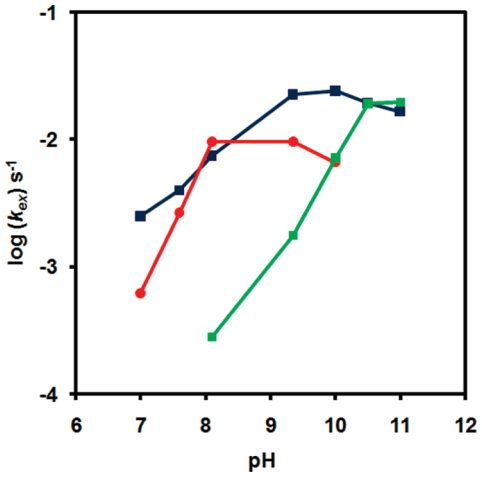

FIGURE 7: Dependence of k_{ex} on pH for wild-type MtOMPDC (blue), D70N (red), and D70G (green) with FUMP.

stability of the carbanion were decreased by the substitution. If rotation about the C_ε−N bond were sufficiently fast, the PIE may increase if the carbanion is then able to discriminate between hydrogen and deuterium. Therefore, we determined the solvent PIEs using FOMP for wild-type MtOMPDC and the D70N and D70G mutants (data not shown). Like wild-type MtOMPDC, the PIEs are 1.0, consistent with the interpretation that the values of k_{ex} measured for the mutants are best explained by the stability of the vinyl carbanion intermediate being independent of the identity of residue 70 (Asp, Asn, or Gly).

Differential Effect of Substitutions for Asp 70 on Decarboxylation and Exchange. In contrast to large decreases in the rate of decarboxylation that accompany substitutions for Asp 70, formation of the FUMP carbanion by abstraction of H6 is unaffected. The differing effects of the substitutions on k_{cat} for decarboxylation and k_{ex} for exchange of H6 provide additional evidence for formation of a carbanion intermediate in a two-step mechanism.

That the substitutions affect the rate of formation of the intermediate from FOMP (k_{cat}) but not from FUMP $(k_{ex})_{max}$ is consistent with Asp 70 enhancing the rate of decarboxylation by substrate destabilization.

Kinetic and Structural Characterization of the D91N Mutant of ScOMPDC. We constructed and both kinetically and structurally characterized the homologous D91N mutant of ScOMPDC. Because the active site residues are conserved, we expected that the D91N mutant of ScOMPDC also would provide similar evidence for the importance of Asp 91 in destabilizing the enzyme−substrate complex.

However, using FOMP as substrate, we were unable to measure values for k_{cat} and K_M; the value of k_{cat}/K_M is 15 $M^{-1}\ s^{-1}$ at pH 7.1 (data not shown). Using FUMP as substrate, we observed no exchange of H6 of FUMP using high concentrations of the D91N mutant and long incubation times. In contrast to the D70N mutant of MtOMPDC, the D91N mutant of ScOMPDC is severely impaired in both the decarboxylation and exchange reactions.

Structures of wild-type ScOMPDC and its D91N mutant were determined in the absence and presence of 6-azaUMP. In the unliganded structures, the 19-residue active site loops adopt the same open conformation (Figure 8, panel A, top row). In the structure of wild-type ScOMPDC complexed with 6-azaUMP (Figure 8, panel A, left structure in bottom row), the loop is closed, sequestering the ligand from the active site, with the

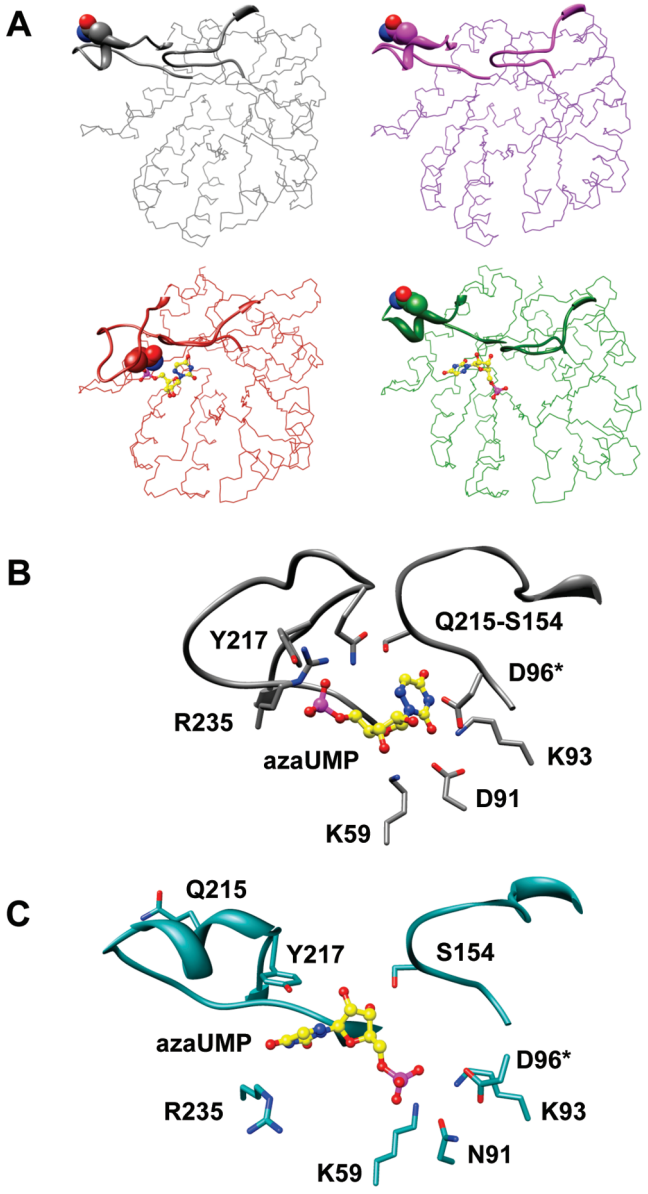

FIGURE 8: Panel A: Comparison of the structures of wild-type ScOMPDC in the absence of ligand (gray), wild-type ScOMPDC complexed with 6-azaUMP (red), the D91N mutant of ScOMPDC in the absence of ligand (magenta), and the D91N mutant of ScOMPDC complexed with 6-azaUMP (green). Panel B: The active site of wild-type ScOMPDC complexed with 6-azaUMP. Panel C: The active site of the D91N mutant complexed with 6-azaUMP.

phosphate group hydrogen-bonded to Gln 215, Tyr 217, and Arg 235, and enforcing the juxtaposition of N6 to the active site hydrogen-bonding network that is reinforced by the Ser 154-Gln 215 "clamp" (*38*). Our structures for wild-type ScOMPDC are similar to those reported previously for the unliganded enzyme and its complex with BMP (*5*).

In the structure of the D91N mutant complexed with 6-azaUMP (Figure 8, panel A, right structure in bottom row), the ligand is bound in the active site. However, the loop in the open conformation and, remarkably, the phosphate and pyrimidine "ends" of the molecule occupy "opposite" positions in the active site relative to the 6-azaUMP ligand in wild-type ScOMPDC (Figure 8, panel B, wild type; panel C, D91N mutant): the phosphate group is hydrogen-bonded to both Lys 59 and Lys 93 in the active site hydrogen-bonded network and the pyrimidine base is proximal to Tyr 217 in the open loop and, also,

Scheme 3

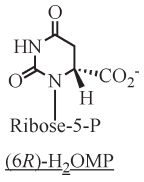

(6*R*)-H_2OMP

Scheme 4

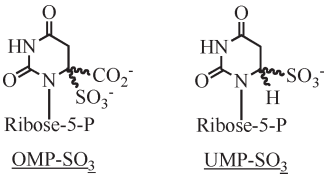

OMP-SO_3 UMP-SO_3

exposed to solvent. To the extent that this structure reflects the geometry of binding of FOMP and FUMP to the D91N mutant, this structure provides an explanation for the inability for the D91N mutant to catalyze decarboxylation of FOMP and exchange of H6 of FUMP.

This structure also provides a possible explanation for Wolfenden's observation that derivatives of OMP and UMP obtained by addition of sulfite to the 5,6 double bond of the pyrimidine bases are effective inhibitors of ScOMPDC, with the values of their K_is lower than that for UMP (Scheme 4) (*23*).

Inhibition by these bulky, anionic substrate/product analogues was used as evidence that substrate destabilization by enforced electrostatic interactions between the substrate carboxylate group and the Asp-Lys-Asp triad cannot be important in producing the large rate acceleration in a "commodious" active site. However, our structure of the D91N mutant with 6-azaUMP strikingly reveals that the active site of ScOMPDC can bind ligands in nonproductive conformations as a result of opportunistic interactions with the conformationally flexible active site loop that provide a structural strategy for avoiding otherwise unfavorable interactions with the Asp-Lys-Asp triad. Perhaps the (6*R*)-diastereomer of UMP-SO_3 can be accommodated in the active site of ScOMPDC as (6*R*)-H_2OMP is accommodated in the active site of MtOMPDC, but it is unlikely that the diastereomers of OMP-SO_3 can be similarly accommodated because of enforced "crowding" of the anionic substituents vis á vis the Asp-Lys-Asp triad.

Role of Asp 70 in Catalysis. The substantial effects of substitutions for Asp 70 on k_2 for decarboxylation (as much as ~2700-fold for D70G with FOMP) relative to the insensitivity of the value of k_{ex} is most simply explained by a two-step mechanism involving the formation of a carbanion intermediate. In this mechanism, the carboxylate side chain of Asp 70 influences the rate of formation of the intermediate (decarboxylation) but not its stability (exchange). This differential effect is consistent with an unfavorable interaction between the carboxylate group of Asp 70 and the orotate carboxylate group that is relieved, in part, by the neutral carboxamide group but, more substantially, by a smaller, uncharged group.

A structural description of the substrate destabilization is uncertain, although the OMP-liganded structure of the D70A/K72A mutant of MtOMPDC has been used as evidence that displacement of the carboxylate group out of the plane of the pyrimidine base may be important for catalysis (*35*). As noted previously and illustrated in Figure 4, in this mutant distortion

occurs despite the absence of the side chains of Asp 70 and Lys 72 that might be expected to provide the electrostatic and steric destabilizing interactions. A hydrogen bond is formed between the out-of-plane OMP carboxylate group and the conserved Lys 42; perhaps this interaction is sufficient to stabilize the observed distorted structure for the substrate.

An unfavorable electrostatic interaction between the carboxylate groups of Asp 70 and OMP may destabilize the enzyme−substrate complex as it proceeds to the transition state for decarboxylation; this interaction is not possible in the exchange reaction. However, that (1) the D70N and D70G substitutions cause small *increases* in the value of K_M for OMP (Table 4) and (2) the K_i for UMP (~0.4 mM) is ~400-fold larger than the K_d for OMP (~1.0 μM) (*39*) show that destabilizing interactions that produce an increase in the value of k_{cat} are not expressed in the measured binding constants.

The destabilizing interactions that promote decarboxylation may develop as the transition state for decarboxylation is approached, perhaps as a result of conformational changes that are coupled to substrate binding (Jiali Gao, personal communication). This strategy for catalysis would require sufficient stabilization of the transition state to overcome the electrostatic destabilization that results from coordinated motion of the anionic carboxylate groups of the OMP substrate and the active site. Both computational and dynamic (NMR) studies of the reaction coordinate can be expected to provide further insights into the structural bases for the substrate destabilization that is suggested by the differential effects of substitution for Asp 70 on decarboxylation of the substrate and exchange of H6 of the product with solvent hydrogen.

Mechanism and Rate Acceleration for the OMPDC-Catalyzed Reaction. Substantial evidence exists for the formation of a carbanion intermediate in the OMPDC-catalyzed reaction: (1) the solvent deuterium product isotope effect is 1.0 (*16*), (2) H6 of the UMP product undergoes exchange with solvent hydrogen (*17*), and (3) as documented in this paper, substitutions for Asp 70 in MtOMPDC influence decarboxylation but not exchange. Thus, the two-step mechanism is secure.

The rate acceleration for the OMPDC-catalyzed reaction is 10^{17}. The rate of exchange of H6 of the UMP product with solvent hydrogen provides an upper limit on the pK_a of the UMP product in the active site ($\leq$22) and, therefore, a lower limit on the stabilization of the carbanion intermediate ($\geq$14 kcal/mol). Thus, stabilization of the carbanion intermediate and the transition state(s) involved in its formation account for a substantial part of the rate acceleration ($\geq 10^{10}$). In principle, all of the rate acceleration could result from stabilization of anionic species in the active site. But, the kinetic and structural data described in this paper provide evidence that substrate destabilization also contributes to the rate acceleration, although whether the contribution is quantitated by the decrease in the value of k_2 observed with D70G (~4.7 kcal/mol) is uncertain.

The structural bases for both stabilization of the vinyl carbanion intermediate and substrate destabilization also are not yet certain. In the case of stabilization of the intermediate, the general acidic Lys 72 in MtOMPDC (Lys 91 in ScOMPDC) has been invoked as providing substantial, and perhaps all of the, stabilization on the basis of the structures of liganded complexes (*35*). However, other factors, including the hydrogen-bonding environment of O4 of the pyrimidine base that could stabilize an anionic carbene intermediate, have not been experimentally investigated (*20*, *21*). In the case of substrate destabilization, Asp 70 has been implicated as important, but whether geometric distortion of the OMP substrate is catalytically relevant remains unknown. These and other issues are under investigation in our laboratories.

REFERENCES

1. Wood, , B. M., Chan, , K. K., Amyes, , T. L., Richard, , J. P., and Gerlt, J. A. (2009) Mechanism of the orotidine 5′-monophosphate decarboxylase-catalyzed reaction: effect of solvent viscosity on kinetic constants, *Biochemistry* (DOI 10.1021/bi9006226).
2. Radzicka, A., and Wolfenden, R. (1995) A proficient enzyme. *Science 267*, 90–93.
3. Miller, B. G., and Wolfenden, R. (2002) Catalytic proficiency: the unusual case of OMP decarboxylase. *Annu. Rev. Biochem. 71*, 847–885.
4. Traut, T. W., and Temple, B. R. (2000) The chemistry of the reaction determines the invariant amino acids during the evolution and divergence of orotidine 5′-monophosphate decarboxylase. *J. Biol. Chem. 275*, 28675–28681.
5. Miller, B. G., Hassell, A. M., Wolfenden, R., Milburn, M. V., and Short, S. A. (2000) Anatomy of a proficient enzyme: the structure of orotidine 5′-monophosphate decarboxylase in the presence and absence of a potential transition state analog. *Proc. Natl. Acad. Sci. U.S.A. 97*, 2011–2016.
6. Wu, N., Mo, Y., Gao, J., and Pai, E. F. (2000) Electrostatic stress in catalysis: structure and mechanism of the enzyme orotidine monophosphate decarboxylase. *Proc. Natl. Acad. Sci. U.S.A. 97*, 2017–2022.
7. Appleby, T. C., Kinsland, C., Begley, T. P., and Ealick, S. E. (2000) The crystal structure and mechanism of orotidine 5′-monophosphate decarboxylase. *Proc. Natl. Acad. Sci. U.S.A. 97*, 2005–2010.
8. Harris, P., Navarro Poulsen, J. C., Jensen, K. F., and Larsen, S. (2000) Structural basis for the catalytic mechanism of a proficient enzyme: orotidine 5′-monophosphate decarboxylase. *Biochemistry 39*, 4217–4224.
9. Miller, B. G., Snider, M. J., Short, S. A., and Wolfenden, R. (2000) Contribution of enzyme-phosphoribosyl contacts to catalysis by orotidine 5′-phosphate decarboxylase. *Biochemistry 39*, 8113–8118.
10. Miller, B. G., Butterfoss, G. L., Short, S. A., and Wolfenden, R. (2001) Role of enzyme-ribofuranosyl contacts in the ground state and transition state for orotidine 5′-monophosphate decarboxylase: A role for substrate destabilization?. *Biochemistry 40*, 6227–6232.
11. Miller, B. G., Snider, M. J., Wolfenden, R., and Short, S. A. (2001) Dissecting a charged network at the active site of orotidine-5′-phosphate decarboxylase. *Biochemistry 40*, 15174–15176.
12. Wu, N., Gillon, W., and Pai, E. F. (2002) Mapping the active site-ligand interactions of orotidine 5′-monophosphate decarboxylase by crystallography. *Biochemistry 41*, 4002–4011.
13. Warshel, A., Strajbl, M., Villa, J., and Florian, J. (2000) Remarkable rate enhancement of orotidine 5′-monophosphate decarboxylase is due to transition-state stabilization rather than to ground-state destabilization. *Biochemistry 39*, 14728–14738.
14. Gao, J. (2003) Catalysis by enzyme conformational change as illustrated by orotidine 5′-monophosphate decarboxylase. *Curr. Opin. Struct. Biol. 13*, 184–192.
15. Feng, W. Y., Austin, T. J., Chew, F., Gronert, S., and Wu, W. (2000) The mechanism of orotidine 5′-monophosphate decarboxylase: catalysis by destabilization of the substrate. *Biochemistry 39*, 1778–1783.
16. Toth, K., Amyes, T. L., Wood, B. M., Chan, K., Gerlt, J. A., and Richard, J. P. (2007) Product deuterium isotope effect for orotidine 5′-monophosphate decarboxylase: evidence for the existence of a short-lived carbanion intermediate. *J. Am. Chem. Soc. 129*, 12946–12947.
17. Amyes, T. L., Wood, B. M., Chan, K., Gerlt, J. A., and Richard, J. P. (2008) Formation and stability of a vinyl carbanion at the active site of orotidine 5′-monophosphate decarboxylase: pKa of the C-6 proton of enzyme-bound UMP. *J. Am. Chem. Soc. 130*, 1574–1575.
18. Sievers, A., and Wolfenden, R. (2002) Equilibrium of formation of the 6-carbanion of UMP, a potential intermediate in the action of OMP decarboxylase. *J. Am. Chem. Soc. 124*, 13986–13987.
19. Yeoh, F. Y., Cuasito, R. R., Capule, C. C., Wong, F. M., and Wu, W. (2007) Carbanions from decarboxylation of orotate analogs: stability and mechanistic implications. *Bioorg. Chem. 35*, 338–343.
20. Lee, J. K., and Houk, K. N. (1997) A proficient enzyme revisited: the predicted mechanism for orotidine monophosphate decarboxylase. *Science 276*, 942–945.
21. Houk, K. N., Lee, J. K., Tantillo, D. J., Bahmanyar, S., and Hietbrink, B. N. (2001) Crystal structures of orotidine monophosphate decarboxylase:

does the structure reveal the mechanism of nature's most proficient enzyme?. *ChemBioChem 2*, 113–118.
22. Callahan, B. P., Bell, A. F., Tonge, P. J., and Wolfenden, R. (2006) A Raman-active competitive inhibitor of OMP decarboxylase. *Bioorg. Chem. 34*, 59–65.
23. Lewis, C. A.Jr., and Wolfenden, R. (2007) Indiscriminate binding by orotidine 5′-phosphate decarboxylase of uridine 5′-phosphate derivatives with bulky anionic C6 substituents. *Biochemistry 46*, 13331–13343.
24. Ames, B. N. (1966) Assay of Inorganic Phosphate, Total Phosphate and Phosphatases. *Methods Enzymol. 8*, pp 115−118.
25. Hruska, F. E. (1971) Molecular conformation of orotidine, a naturally occurring nucleoside, in syn conformation in aqueous solution. *J. Am. Chem. Soc. 93*, 1795–1797.
26. Fujita, K., Matsukawa, A., Shibata, K., Tanaka, T., Taniguchi, M., and Oi, S. (1994) Synthesis of 5-fluorouridine 5′-diphosphate galactose from 5-fluorouridine by chemical phosphorylation and microbial uridylyl transfer. *Carbohydr. Res. 265*, 299–302.
27. Otwinowski, Z., Minor, W. (1997) Processing of X-ray diffraction data collected in oscillation mode, in *Methods in Enzymology* (Carter, C. W. J., Sweet, R. M., Abelson, J. N., and Simon, M. I., Eds.) pp 307−326, Academic Press, New York.
28. Long, F., Vagin, A. A., Young, P., and Murshudov, G. N. (2008) BALBES: a molecular-replacement pipeline. *Acta Crystallogr., Sect. D: Biol. Crystallogr. 64*, 125–132.
29. Jones, A. T. (1985) Interactive computer graphics: FRODO. *Methods Enzymol. 115*, 157–171.
30. Brunger, A. T., Adams, P. D., Clore, G. M., DeLAno, W. L., Gros, P., Grosse-Kunstleve, R. W., Jiang, J. S., Kuszewski, J., Nilges, M., Pannu, N. S., Read, R. J., Rice, L. M., Simonson, T., and Warren, G. L. (1998) Crystallography & NMR system: A new software suite for macromolecular structure determination. *Acta Crystallogr. D54*, 905–921.
31. Lamzin, V. S., and Wilson, K. S. (1993) Automated refinement of protein models. *Acta Crystallogr., Sect. D: Biol. Crystallogr. 49*, 129–147.
32. CCP4 (1994) The CCP4 suite: Programs for protein crystallography. *Acta Crystallogr. D50*, 760–763.
33. Pettersen, E. F., Goddard, T. D., Huang, C. C., Couch, G. S., Greenblatt, D. M., Meng, E. C., and Ferrin, T. E. (2004) UCSF Chimera—a visualization system for exploratory research and analysis. *J. Comput. Chem. 25*, 1605–1612.
34. Shostak, K., and Jones, M. E. (1992) Orotidylate decarboxylase: insights into the catalytic mechanism from substrate specificity studies. *Biochemistry 31*, 12155–12161.
35. Van Vleet, J. L., Reinhardt, L. A., Miller, B. G., Sievers, A., and Cleland, W. W. (2008) Carbon isotope effect study on orotidine 5′-monophosphate decarboxylase: support for an anionic intermediate. *Biochemistry 47*, 798–803.
36. Sievers, A., and Wolfenden, R. (2005) The effective molarity of the substrate phosphoryl group in the transition state for yeast OMP decarboxylase. *Bioorg. Chem. 33*, 45–52.
37. Amyes, T. L., Richard, J. P., and Tait, J. J. (2005) Activation of orotidine 5′-monophosphate decarboxylase by phosphite dianion: the whole substrate is the sum of two parts. *J. Am. Chem. Soc. 127*, 15708–15709.
38. Barnett, S. A., Amyes, T. L., Wood, B. M., Gerlt, J. A., and Richard, J. P. (2008) Dissecting the total transition state stabilization provided by amino acid side chains at orotidine 5′-monophosphate decarboxylase: a two-part substrate approach. *Biochemistry 47*, 7785–7787.
39. Porter, D. J., and Short, S. A. (2000) Yeast orotidine-5′-phosphate decarboxylase: steady-state and pre-steady-state analysis of the kinetic mechanism of substrate decarboxylation. *Biochemistry 39*, 11788–11800.